Metamaterial Platforms for Spintronic Modulation of Mid-Infrared Response under Very Weak Magnetic Field

Gaspar Armelles,*,[†] Luca Bergamini,[‡,§] Nerea Zabala,[‡,§] Fernando García,[†] Maria Luisa Dotor,[†] Lorena Torné,[†] Raquel Alvaro,[†] Amadeu Griol,[∥] Alejandro Martínez,[∥] Javier Aizpurua,[‡] and Alfonso Cebollada*,[†]

[†]Instituto de Micro y Nanotecnología (IMN-CNM), CSIC (CEI UAM+CSIC), Isaac Newton, 8, Tres Cantos 28760, Madrid, Spain
[‡]Materials Physics Center, CSIC-UPV/EHU and DIPC, San Sebastian 20018, Spain
[§]Department of Electricity and Electronics, FCT-ZTF, UPV-EHU, Bilbao 48080, Spain
[∥]Nanophotonics Technology Center, Universitat Politècnica de València, Camino de Vera s/n, Valencia 46022, Spain

ⓢ Supporting Information

ABSTRACT: In this work, we experimentally demonstrate magnetic modulation of mid-infrared (mid-IR) plasmon resonances in microantenna and hole-array metamaterial platforms made of $Ni_{81}Fe_{19}$/Au multilayers. The responsible mechanism is the magnetorefractive effect linked to the giant magnetoresistance (GMR) present in this system. $Ni_{81}Fe_{19}$/Au multilayers experience a modification in the electrical resistivity upon the application of a small magnetic field. This directly translates into a change in the optical constants of the multilayer, making it possible to magnetically modulate the plasmon resonances. Because GMR acts on conduction electrons, the optical modulation occurs in the low energy, mid-IR range, even being possible to extend it to the THz range. Electrodynamical calculations confirm the experimental observations. This approach improves by up to 2 orders of magnitude previous attempts for mid-IR magnetic modulation, is potentially ultrafast due to the characteristic spintronics dynamics, and establishes a roadmap for spintronically controlled devices in the whole mid-IR to THz band.

KEYWORDS: mid-infrared, magnetic modulation, magnetorefractive, spintronics, plasmonics
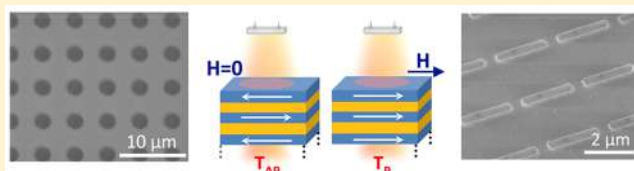
Magnetic systems are characterized by a number of properties that can be controlled by the application of a magnetic field. For example, their interaction with light can be easily manipulated in the visible and near infrared (IR) regimes by exploiting the magneto-optical effect (MOE) responsible for the magnetic dependence of the off-diagonal elements of the dielectric tensor (by MOE, we refer to all possible configurations of incidence and collection of light with generality). This is the case for many ferromagnetic materials, where the MOE is sizable and achievable at low magnetic fields. Combining this effect with plasmon resonances has recently allowed for a number of active magneto-plasmonic platforms[1−7] where both magnetic and plasmonic functionalities are strongly intertwined. Unfortunately, in these plasmonic platforms, the MOE effect decreases in the IR and beyond, where the optical properties of metals are mainly dominated by conduction electrons. On the other hand, if semiconductor instead of metallic platforms are considered, surface magneto plasmons can be exploited for potential applications at infrared frequencies, but this requires magnetic field intensities of ∼1 T, which can hinder many applications.[8] An alternative way to magnetically act on the IR response of ferromagnetic structures is to use the dependence of the DC conductivity on the electron spin. This is the basis of spin electronics or spintronics, a discipline of relatively short history

but huge technological impact, and whose most representative effect is the giant magnetoresistance (GMR).[9,10] This effect stems from the dependence of the resistivity of a system on the relative orientation of the electron spin and the local magnetization. A typical example is a metallic multilayer composed of ferromagnetic layers (in our case $Ni_{81}Fe_{19}$) separated by nonferromagnetic spacers (in our case Au) (Figure 1, center). The electrical resistivity of the system is different if the $Ni_{81}Fe_{19}$ layer magnetizations are oriented parallel (ρ_P) or antiparallel (ρ_{AP}) (Figure 1a), and thus, moderate magnetic fields are able to produce sizable changes in resistivity,[11] as shown in Figure 1a.

The spin-dependent electron transport properties of a material are genuinely expressed in the GMR effect. However, this dependency is also responsible for a broad-band change in the polarizability via the so-called magnetorefractive effect (MRE),[12,13] consisting of the change in the diagonal elements of the dielectric tensor due to the magnetic field-induced change in the electrical resistivity (Figure 1b) (see Supporting Information). Actually, $Ni_{81}Fe_{19}$/Au multilayers exhibit MRE at very low fields and therefore are excellent candidates for plasmon modulation in the mid-IR.[14] In addition, the magnetic
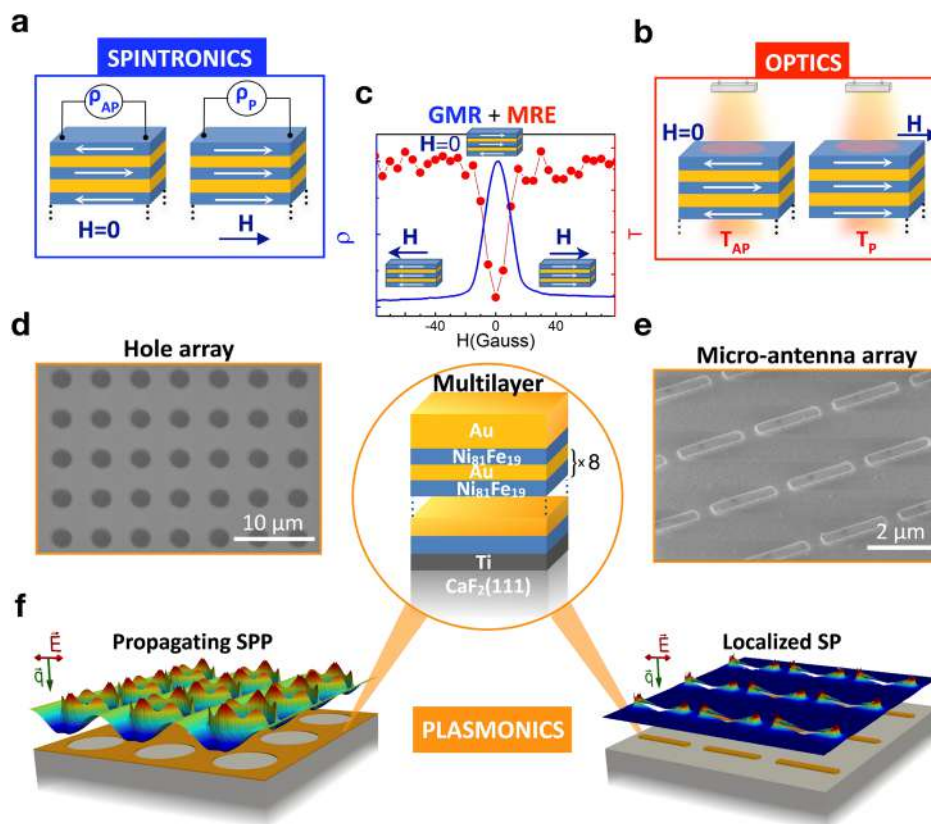
Figure 1. A $Ni_{81}Fe_{19}$/Au multilayer with specific Au spacer thickness exhibits magnetic field-controlled spintronic (GMR) and mid-IR (MRE) optical properties, allowing plasmon modulation in hole and microantenna arrays. (a) An external magnetic field H reorients the individual $Ni_{81}Fe_{19}$ layer magnetizations from antiparallel to parallel configurations with the subsequent change in the electrical resistivity (GMR). (b) The magnetic field-induced change in resistivity produces a change in the mid- and far-IR optical properties (MRE) dominated by conduction electrons (T_P and T_{AP} correspond to the trasnmission when the $Ni_{81}Fe_{19}$ layer magnetizations are oriented parallel or antiparallel, respectively). (c) Being directly correlated, both GMR and MRE exhibit linked magnetic field dependence. (d, e) Metamaterial platforms capable of presenting propagating (d) and localized (e) plasmons are easily obtained by fabricating hole and microantenna arrays out of multilayered continuous films. Because of the spin-dependent scattering time of the electrons, the resistivity depends on the relative orientations of the spin of the electron and the ferromagnetic layer magnetizations. (f) These resonant excitations are susceptible to magnetic modulation via MRE control of the material's optical constants.

field dependence of GMR and MRE allows for an experimental verification of their direct correlation (Figure 1c). For the MRE effect to be efficiently transferred into an enhanced modulated-optical response, structures showing plasmonic resonances and thus exhibiting strong light−matter interaction appear as best-suited candidates.

Here, we demonstrate light modulation via GMR in two different metasurfaces composed by the repetition of magneto-refractive metallic units (substructured in nonferromagnetic-ferromagnetic layers) in square-lattice arrays. The optical properties of these metamaterials combine the magneto-refractive response of the units (supporting highly confined plasmons at mid-IR wavelengths) with the metamaterial response of the array producing diffraction. We consider two canonical structures: an array of holes enabling extraordinary optical transmission (EOT) (magnetorefractive response given by the layered film surrounding the hole units, Figure 1d)[15,16] and an array of dipole-like optical antennas (magnetorefractive response given by the layered structure forming the antenna itself, Figure 1e).[17−19] Remarkably, as will be shown in this paper, the mid-IR plasmon response associated with these spintronic metamaterial platforms (depicted in Figure 1f) experiences large intensity modulation under the application of a very small magnetic field.

RESULTS AND DISCUSSION

For the hole array platform, two $Ni_{81}Fe_{19}$/Au multilayers with 3.8% and 0% GMR, respectively, were deposited and then perforated using ultraviolet lithography or focused ion beam milling. For tuning the GMR in this system, it is necessary to have atomic level control of the Au spacer thickness because variations of just 0.5 nm can make GMR drop from a sizable value to zero.[11] In this work, this control is achieved by exact calibration of the different materials sources and cross checking with X-ray techniques (see Supporting Information section 1). In this way, identical squared arrays of holes with 2.7 μm diameter and 5 μm period supporting propagating plasmons in the 3−10 μm spectral range were created.

Mid-IR transmission spectra are obtained for p polarization, as depicted in Figure 2a (see Supporting Information section 6 for s polarization) for both 3.8% and 0% GMR multilayered hole arrays. The transmission spectra in the absence of magnetic field are presented in Figure 2b (upper left), where both types of MLs show almost identical transmission.

This effect can be understood due to the similarity of the hole patterns with only a small difference in the Au content between both structures. The observed peaks correspond to the excitation of propagating plasmons in the ML−air and ML−substrate interfaces (see the corresponding induced
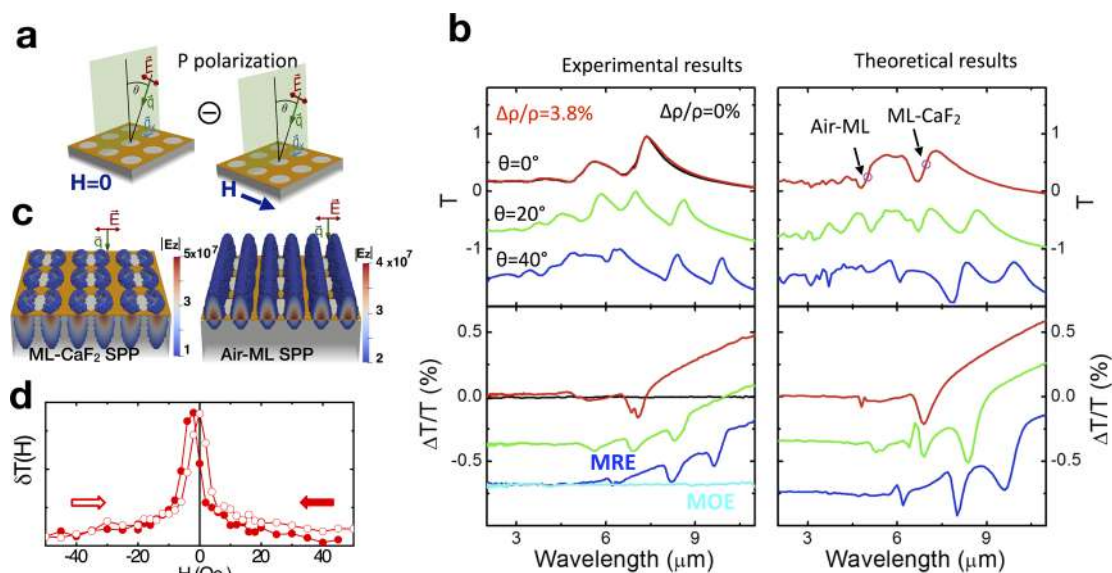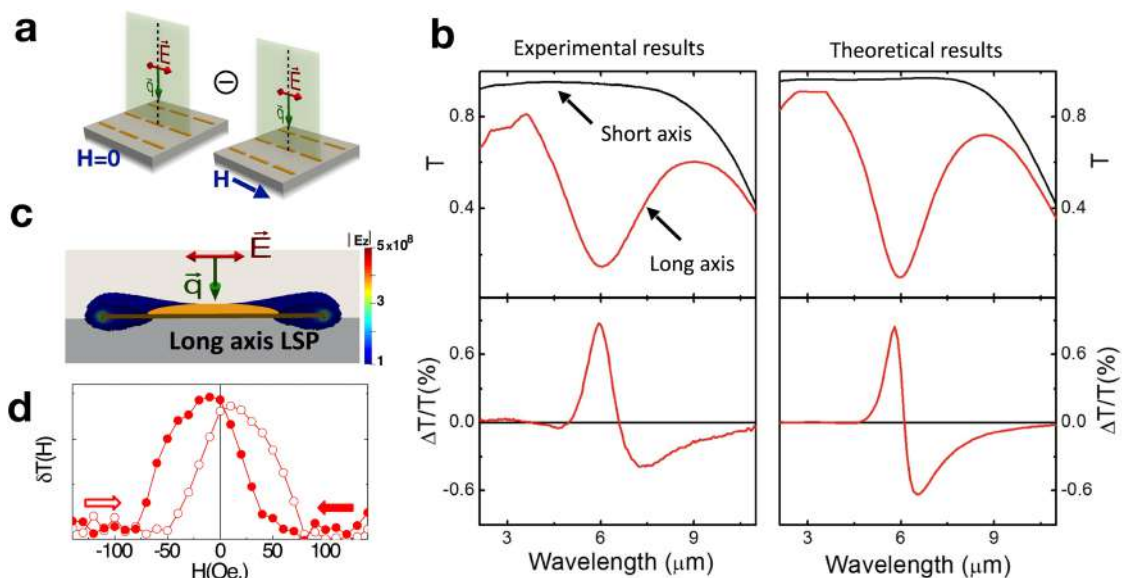
Figure 2. Propagating plasmons in hole array spintronic platforms are modulated by a small external magnetic field. (a) Excitation configuration for p-polarized transmission and magnetic modulation. (b) Experimental and theoretical transmissions show excitation of propagating resonant modes at the multilayer−substrate and −air interfaces, both with characteristic dispersion. Experimental transmission at normal incidence for identical platforms fabricated out of a 3.8% (red curve) and a 0% (black curve) GMR multilayer are indistinguishable. The corresponding magnetic modulation of the transmission shows clear derivative-like features corresponding with the excited modes. The experimental comparison of the MRE (dark blue) and MOE (light blue) demonstrates that the former is dominant in this spectral range. All the spectra at different angles are vertically shifted for clarity. (c) Theoretically determined fields for the modes excited at the multilayer−substrate (at $\lambda = 7 \ \mu$m) and −air (at $\lambda = 5 \ \mu$m) interfaces. (d) Magnetic field dependence of the difference between the transmission when the sample is saturated in the positive direction, $T(M_{sat})$, and the transmission at the value of the magnetic field, $T(H)$: $\delta T = \delta T(H) = T(M_{sat}) - T(H)$ (to increase the signal-to-noise ratio, we present this difference summed at different wavelengths). Solid symbols: the magnetic field goes from positive to negative values; open symbols: the magnetic field goes from negative to positive values. The shape and magnetic field behavior are identical to the corresponding GMR curve (see Figure S3a), confirming the spintronic origin of the mid-IR modulation and its persistence upon the microfabrication process.

plasmonic near-field patterns calculated in Figure 2c). The dispersion of the plasmon-polariton peaks can be traced by varying the angle of incidence (0°, 20°, and 40°). A detailed analysis of these peaks is contained in Supporting Information section 7. Theoretical transmission spectra (Figure 2b (upper right)) nicely reproduce the position, intensity, and dispersion of the EOT peaks. We can now explore the MRE in each of the configurations by analyzing the modification of the transmission associated with differences in plasmon excitation. To this end, we apply a weak magnetic field, producing either high (0 Oe) or low (30 Oe) platform resistivity, respectively. The change in transmission, normalized to the transmission at magnetic saturation (low resistivity state), for the spintronic metamaterial at different incidence angles is shown in Figure 2b (lower left). Note that each feature observed in the transmission spectra and corresponding to the excitation of a plasmonic mode finds its counterpart in the magnetic-modulated spectra in a derivative-like fashion, indicative of a magnetic field-induced modulation of the transmission features. This modulation lies in the magnetic field control of the plasmon wavevector via modification of the refractive index and as a consequence of its excitation conditions. Further evidence of the magnetorefractive origin of the observed modulation can be drawn by simply characterizing in a similar fashion the ML with no GMR. As shown in Figure 2b (lower left), the corresponding black curve shows no modulation in this ML where GMR, and therefore MRE, are absent. To confirm this mechanism, we perform numerical electrodynamical calculations (Figure 2b (lower right)) that reproduce all of the experimental trends. A possible source for the minor qualitative discrepancies, mainly in terms of

intensity and width of spectral features, is obviously due to the intrinsic structural defects inherent to the actual fabricated samples (interface or surface roughness or morphological imperfections) not considered in the calculations. Further confirmation of the magnetoresistive origin of this mechanism can be traced by representing the magnetic field dependence of the magnetic modulation. The resulting data are plotted on Figure 2d, showing identical shape to that of the corresponding GMR curve of the holed membrane (Figure S3a).

Furthermore, this spintronic metamaterial platform allows for a direct comparison of the magnitude of both MRE and MOE under the very same experimental conditions for the mid-IR spectral range. For off-normal incidence, both MRE and MOE appear as a change in the transmission, $\Delta T_{MOE}/T$: $(T(M_{sat}) - T(-M_{sat}))/(T(M_{sat}) + T(-M_{sat}))$, $\Delta T_{MRE}/T$: $(T(M_{sat}) - T(0))/T(0)$ (comparison at normal incidence is not possible because the MOE with this magnetic configuration is zero at normal incidence).[20] We show this comparison for a 40° incidence angle in Figure 2b (lower left), where the MOE (light blue curve) is clearly much weaker than the MRE (dark blue) in this spectral range.

Complementary to the modulation of surface plasmon polaritons, we also explore the possibility of obtaining mid-IR modulation from localized excitations in microparticles. To that end, we fabricate a platform consisting of a set of dipole-like optical antennas supporting localized surface plasmons. Similar to the previous architecture, $Ni_{81}Fe_{19}/Au$ continuous multilayers, in this case with 4% GMR, are patterned by electron beam lithography and Ar ion etching. The resulting structures are square arrays (2.6 μm period) of optical

Figure 3. Localized plasmons in microantenna array spintronic platforms are modulated by a small external magnetic field. (a) Excitation configuration for p-polarized transmission and magnetic modulation. (b) Experimental (left panels) and theoretical (right panels) transmissions (upper panels) show excitation of localized mode along the long axis of the antennas. The corresponding magnetic modulation of the transmission (lower panels) shows clear derivative-like shape of the excited mode. (c) Theoretically determined fields for the excited microantenna mode (at λ =6 μm). (d) Magnetic field dependence of the difference between the transmission when the sample is saturated in the positive direction, $T(M_{sat})$, and the transmission at the value of the magnetic field, $T(H)$: $\delta T = \delta T(H) = (T(M_{sat}) - T(H))$ (to increase the signal-to-noise ratio, we present this difference summed at different wavelengths). Solid symbols: the magnetic field goes from positive to negative values; open symbols: the magnetic field goes from negative to positive values. The shape and magnetic field behavior is identical to a typical GMR curve, confirming the spintronic origin of the mid-IR modulation and its persistence upon the microfabrication process.

antennas with in-plane dimensions of 2 × 0.3 μm and 60 nm thick (see SEM image in Figure 1e).

With incident light polarized parallel to the long axis (Figure 3a), the transmission through the array of dipolar antennas shows a clear dip at a wavelength of ∼6 μm (Figure 3b (upper left)), which indicates the excitation of an electric dipolar resonance along the long rod axis. The localized dipolar pattern induced in the antennas is shown in Figure 3c. When the incident light is polarized along the short axis, no spectral features are observed in this spectral range. Numerical results that consider the main geometrical features of the antenna array reproduce accurately the properties of the plasmon excitation, as shown in Figure 3b (upper right).

We explore now the magnetic modulation of these localized plasmon resonances with the use of the same experimental setup. To allow for full magnetic saturation of the rods, the magnetic field is applied onto the rod plane and along the long antennas axis as determined by transverse MOE loops using a green laser. The magnetic-modulated transmission spectrum for light polarized along the long antennas axis across the array showing a 4% ML GMR is shown in Figure 3b (lower left). The dip-like aspect of the transmission becomes a derivative-like feature. In this case, the MRE-induced change in the refractive index of the material produces a slight shift in the energy of the localized plasmon mode in the ML antenna, and as a consequence, a derivative shape in the $\Delta T/T$ spectrum is apparent. Similar to the hole-array platform, having access to the experimentally measured optical constants for the high and low electrical resistivity states allows for obtaining a theoretical estimation of the expected magnetic modulation, as shown in Figure 3b (lower right), showing excellent agreement with experiments.

Finally, confirmation of the magnetoresistive origin of this effect can also be traced in this case by observing the modulated response as a function of the applied magnetic field. This quantity is shown in Figure 3d, which also resembles the functional dependence of the GMR effect and the observable hysteresis. In our case, it is not possible to directly measure the GMR of the antennas as it would require applying electrical contacts. However, and in addition to the obtained typical GMR shape shown in Figure 3d, MOE hysteresis loops measured for the antennas in the visible region (Figure S4) demonstrate the enhancement of the saturation fields as a continuous film is patterned down to an antenna array with saturation field values similar to those in Figure 3d. All this strongly points to the fact that GMR characteristics of the original ML material are still present in the antennas after patterning.

As mentioned, the physical mechanism responsible for this modulation is the magnetic field control of the complex refractive index of the spintronic multilayers via the MRE. The modulation of mid-IR plasmon resonances is then experimentally determined and theoretically confirmed through magnetic modulation measurements of the transmission of both hole- and antenna-array platforms. In both cases, the correlation between the plasmon-related transmission features and the modulation transmission ones is obvious. Interestingly, maxima in the modulation transmission occur for minima in the transmission in antenna-arrays and for high-slope regions in the hole-arrays. This difference is very likely due to the different nature of the excited resonances: on one hand with surface plasmon polaritons indirectly dependent on refractive index changes via their wavevector, and localized plasmons on the other hand directly dependent on the refractive index. In both cases, irrespective of happening at a minimum or an

intermediate transmission region, the signal-to-noise obtained in the modulation of the response is large and of extremely good quality, thus opening the path to broad-band optical engineering applications controlled by magnetic fields.

As magnetic-metallic multilayers show the same underlying physics responsible for the magnetotransport properties discussed here also in the THz range,[21] it is expected that a similar dependence of the optical properties on the magnetic field could be found at this frequency range; thus, our metamaterial structures could set the basis for future modulation of THz response by magnetic fields.

To summarize, using multilayered platforms based on spintronic metamaterials, we have shown that it is possible to significantly modulate plasmon resonances in the mid-IR by simply applying low-intensity external magnetic fields. The modulation is sizable and with excellent signal-to-noise ratio, and the material platforms as well as the experimental setup are of simple realization. Besides its impact in the mid-IR regime, this modulation mechanism, based on the GMR-driven control of optical properties, occurs in a low-energy electromagnetic range and therefore could easily be extended to the THz, where efficient devices for dynamic light manipulation and modulation are still lacking. Even more, ultrahigh modulation speeds are in principle expected as a result of the high-frequency dynamics of the magnetization reversal involved in the GMR. This approach beats previous attempts for MIR magnetic modulation. For example, in comparison to graphene,[22,23] our approach has a figure of merit (modulation per magnetic field unit) of up to 2 orders of magnitude larger, thus establishing a roadmap for spintronically controlled devices in the whole MIR to THz band.

■ MATERIALS AND METHODS

Deposition, Characterization, and Fabrication. The multilayers were grown on CaF_2 (111) substrates at 150 °C. A 3 nm Ti buffer layer grown by electron beam evaporation was followed by nine layers of $Ni_{81}Fe_{19}$ spaced by eight layers of Au, both deposited by magnetron sputtering from individual $Ni_{81}Fe_{19}$ and Au targets. Typical individual layer thicknesses are 2.9 nm for $Ni_{81}Fe_{19}$ and between 1.9 and 3.3 nm for Au. Finally, a 5 nm Au capping layer was deposited. X-ray diffraction and reflectometry measurements were performed in a multipurpose four-circles diffractometer with Cu $K\alpha$ radiation. Transverse magneto-optic Kerr effect (MOKE) hysteresis loops were recorded using a laser source ($\lambda = 532$ nm) and an electromagnet with sufficient magnetic field to saturate the structures in the field plane. DC magnetoresistance was measured at room temperature using four in-line probes with 2 mA input current and two magnetic coils with enough magnetic field to saturate the samples. Spectral IR characterization was performed in a Bruker VERTEX 70 FTIR spectrometer with a mercury cadmium telluride (MCT) photovoltaic detector and magnetic coils in the samples enclosure, generating sufficient magnetic field to saturate most of the structures. As the thickness of the $Ni_{81}Fe_{19}$ and Au layers are much smaller than the wavelength of light, the multilayer can be considered as an effective medium. This effective dielectric constant of the multilayer for the two magnetic states was obtained from transmission and reflectivity measurements. Combined use of ultraviolet (UV), electron beam, and focused ion beam lithography and Ar ion etching was employed to fabricate the different platforms.

Numerical Simulations. The optical transmissions (T) and differential transmissions ($\Delta T/T$) presented in this work were obtained via electrodynamic calculations by means of the COMSOL Mutiphysics software.[24] The geometry of the systems, as well as the illumination condition and the material permittivities, were all inferred from the experimental setup and characterization. A comprehensive description of all the simulation details is provided in the Supporting Information.

■ ASSOCIATED CONTENT

Ⓢ Supporting Information

The Supporting Information is available free of charge on the ACS Publications website at DOI: 10.1021/acsphotonics.8b00866.

> Description of the structural, magnetic, morphological, and optical characterizations of the continuous films and fabricated structures using best-suited techniques, description of the theoretical calculations along with comparative experimental-vs-calculated results and a study of the holed membrane modes, and derivative-like features of the magnetic modulation as well as a brief description of the correlation between GMR and MRE effects (PDF)

■ AUTHOR INFORMATION

Corresponding Authors
*E-mail: Gaspar.Armelles@csic.es.
*E-mail: Alfonso.Cebollada@csic.es.

ORCID ⓘ
Gaspar Armelles: 0000-0002-2563-1621
Nerea Zabala: 0000-0002-1619-7544
Alejandro Martínez: 0000-0001-5448-0140
Alfonso Cebollada: 0000-0003-1990-4520

Author Contributions

A.C. and G.A. conceived the idea and the experiments and wrote the first version of the manuscript. A.C. grew and characterized the structure, MO hysteresis loops and transport properties of the multilayers, the MO hysteresis loops and transport properties of the hole structures and the MO hysteresis loops of the antennas and analyzed the results. G.A. performed the zero field and field-dependent FTIR measurements and analyzed the results. F.G. designed and set up the experimental GMR system and performed the automation and computer control of the magnetic field-dependent FTIR measurements. M.L.D. coordinated the design of the masks for the holes and the Ar etching of the platforms. R.A. and L.T. performed the Ar etching and AFM and SEM characterization of most of the structures. L.B., N.Z., and J.A. developed all of the numerical calculations in the paper, discussed the concept, and participated in manuscript writing. A.M. and A.G. performed the lithography of the samples. A.M. also carried out preliminary theoretical calculations and participated in the discussion of the results and in manuscript writing.

Notes
The authors declare no competing financial interest.

■ ACKNOWLEDGMENTS

■ REFERENCES

(1) Temnov, V. V.; Armelles, G.; Woggon, U.; Guzatov, D.; Cebollada, A.; Garcia-Martin, A.; Garcia-Martin, J. M.; Thomay, T.; Leitenstorfer, A.; Bratschitsch, R. Active magneto-plasmonics in hybrid metal−ferromagnet structures. *Nat. Photonics* **2010**, *4*, 107−111.

(2) Chin, J. Y.; Steinle, T.; Wehlus, T.; Dregely, D.; Weiss, T.; Belotelov, V. I.; Stritzker, B.; Giessen, H. Nonreciprocal plasmonics enables giant enhancement of thin-film Faraday rotation. *Nat. Commun.* **2013**, *4*, 1599.

(3) Zayets, V.; Saito, H.; Ando, K.; Yuasa, S. Optical Isolator Utilizing Surface Plasmons. *Materials* **2012**, *5*, 857−871.

(4) Davoyan, A. R.; Engheta, N. Nonreciprocal rotating power flow within plasmonic nanostructures. *Phys. Rev. Lett.* **2013**, *111*, 047401.

(5) Armelles, G.; Cebollada, A.; García-Martín, A.; González, M. U. Magnetoplasmonics: Combining magnetic and plasmonic functionalities. *Adv. Opt. Mater.* **2013**, *1*, 10−35.

(6) Maccaferri, N.; Gregorczyk, K. E.; de Oliveira, T. V. A. G.; Kataja, M.; van Dijken, S.; Pirzadeh, Z.; Dmitriev, A.; Åkerman, J.; Knez, M.; Vavassori, P. Ultrasensitive and label-free molecular-level detection enabled by light phase control in magnetoplasmonic nanoantennas. *Nat. Commun.* **2015**, *6*, 6150.

(7) Kuzmin, D. A.; Bychkov, I. V.; Shavrov, V. G.; Temnov, V. V. Plasmonics of magnetic and topological graphene-based nanostructures. *Nanophotonics* **2018**, *7*, 597−611.

(8) Hu, B.; Zhang, Y.; Wang, Q. J. Surface magneto plasmons and their applications in the infrared frequencies. *Nanophotonics* **2015**, *4*, 383−396.

(9) Baibich, M. N.; Broto, J. M.; Fert, A.; Nguyen Van Dau, F.; Petroff, F.; Etienne, P.; Creuzet, G.; Friederich, A.; Chazelas, J. Giant magnetoresistance of (001)Fe/(001)Cr magnetic superlattices. *Phys. Rev. Lett.* **1988**, *61*, 2472−2475.

(10) Binasch, G.; Grünberg, P.; Saurenbach, F.; Zinn, W. Enhanced magnetoresistance in layered magnetic structures with antiferromagnetic interlayer exchange. *Phys. Rev. B: Condens. Matter Mater. Phys.* **1989**, *39*, 4828−4830.

(11) Parkin, S. S. P.; Farrow, R. F. C.; Marks, R. F.; Cebollada, A.; Harp, G. R.; Savoy, R. J. Oscillations of interlayer exchange coupling and giant magnetoresistance in (111) oriented permalloy/Au multilayers. *Phys. Rev. Lett.* **1994**, *72*, 3718−3721.

(12) Jacquet, J. C.; Valet, T. A. A new magnetooptical effect discovered on magnetic multilayers: the magnetorefractive effect. *MRS Online Proc. Libr.* **1995**, *384*, 477−490.

(13) Vopsaroiu, M.; Stanton, T.; Thomas, O.; Cain, M.; Thompson, S. M. Infrared metrology for spintronic materials and devices. *Meas. Sci. Technol.* **2009**, *20*, 045109.

(14) Armelles, G.; Cebollada, A.; García, F.; Pecharromán, C. Magnetic modulation of mid-infrared plasmons using giant magnetoresistance. *Opt. Express* **2017**, *25*, 18784−18796.

(15) Ebbesen, T. W.; Lezec, H. J.; Ghaemi, H. F.; Thio, T.; Wolff, P. A. Extraordinary optical transmission through sub-wavelength hole arrays. *Nature* **1998**, *391*, 667−669.

(16) Ortuño, R.; García-Meca, C.; Rodríguez-Fortuño, F. J.; Håkansson, A.; Griol, A.; Hurtado, J.; Ayucar, J. A.; Bellieres, L.; Rodríguez, P. J.; López-Royo, F.; Martí, J.; Martínez, A. Midinfrared filters based on extraordinary optical transmission through sub-wavelength structured gold films. *J. Appl. Phys.* **2009**, *106*, 124313.

(17) Neubrech, F.; Pucci, A.; Cornelius, T. W.; Karim, S.; Garcia-Etxarri, A.; Aizpurua, J. Resonant Plasmonic and Vibrational Coupling in a Tailored Nanoantenna for Infrared Detection. *Phys. Rev. Lett.* **2008**, *101*, 157403.

(18) Novotny, L.; van Hulst, N. Antennas for light. *Nat. Photonics* **2011**, *5*, 83−90.

(19) Weber, D.; Albella, P.; Alonso-González, P.; Neubrech, F.; Gui, H.; Nagao, T.; Hillenbrand, R.; Aizpurua, J.; Pucci, A. Longitudinal and transverse coupling in infrared gold nanoantenna arrays: long range versus short range interaction regimes. *Opt. Express* **2011**, *19*, 15047−15061.

(20) Belotelov, V. I.; Akimov, I. A.; Pohl, M.; Kotov, V. A.; Kasture, S.; Vengurlekar, A. S.; Gopal, A. V.; Yakovlev, D. R.; Zvezdin, A. K.; Bayer, M. Enhanced magneto-optical effects in magnetoplasmonic crystals. *Nat. Nanotechnol.* **2011**, *6*, 370−376.

(21) Jin, Z.; Tkach, A.; Casper, F.; Spetter, V.; Grimm, H.; Thomas, A.; Kampfrath, T.; Bonn, M.; Kläui, M.; Turchinovich, D. Accessing the fundamentals of magnetotransport in metals with terahertz probes. *Nat. Phys.* **2015**, *11*, 761−766.

(22) Crassee, I.; Levallois, J.; Walter, A. L.; Ostler, M.; Bostwick, A.; Rotenberg, E.; Seyller, T.; van der Marel, D.; Kuzmenko, A. B. Giant Faraday rotation in single and multilayer graphene. *Nat. Phys.* **2011**, *7*, 48−51.

(23) Zanotto, S.; Lange, C.; Maag, T.; Pitanti, A.; Miseikis, V.; Coletti, C.; Degl'Innocenti, R.; Baldacci, L.; Huber, R.; Tredicucci, A. Magneto-optic transmittance modulation observed in a hybrid graphene−split ring resonator terahertz metasurface. *Appl. Phys. Lett.* **2015**, *107*, 121104.

(24) COMSOL Inc. COMSOL Multiphysics. https://www.comsol.com (accessed September 19, 2018).